



# The enhancement of photocatalytic hydrogen production via $Ti^{3+}$ self-doping black $TiO_2/g-C_3N_4$ hollow core-shell nano-heterojunction

Jiaqi Pan, Zongjun Dong, Beibei Wang, Ziyuan Jiang, Chuang Zhao, Jingjing Wang, Changsheng Song, Yingying Zheng, Chaorong Li\*

Department of Physics, and Key Laboratory of ATM&MT Ministry of Education, Zhejiang Sci-Tech University, Hangzhou, 310018, PR China



## ARTICLE INFO

### Keywords:

Photocatalytic hydrogen production  
Black  $TiO_2$   
Nano-heterojunction  
 $Ti^{3+}$  self-doping

## ABSTRACT

The  $Ti^{3+}$  self-doping  $B-TiO_2/g-C_3N_4$  hollow core-shell nano-heterojunction is synthesized via the continuous hydrothermal deposition and sculpture-reduction processes. The results of SEM, XRD, TEM, XPS and FT-IR imply that the  $B-TiO_2/g-C_3N_4$  hollow core-shell nanospheres have been prepared successfully. The photocatalytic activity of the  $B-TiO_2/g-C_3N_4$  nano-heterojunctions remarkably exhibits an enhancement of 18 times and 65 times than that of normal  $TiO_2$  and  $g-C_3N_4$ , respectively. Further, the photocatalytic process and the mechanism of the photocatalytic hydrogen production enhancement have been studied, which could be ascribed to the  $O_v-Ti^{3+}$  in the  $B-TiO_2$  and interface nano-heterojunction, that have been proved by the transient photocurrent, PL, EIS and Mott-Schottky plots.

## 1. Introduction

The hydrogen ( $H_2$ ), with the green-renewability and high energy density, is expected as the most promising candidate in the exploitation of energy resources. To date, lots of inspiring ways have been achieved, such as chemical, physical or electrocatalytic hydrogen production [1–3], etc. Among these researches, the photocatalytic hydrogen production [4,5], owns the clean, cheap and environmental performance, have be the current focus of the hydrogen energy exploitation. So far, lots of materials have been reported with the remarkable photocatalytic hydrogen production performance, such as  $ZnO$  [6],  $MoS_2$  [7],  $SrTiO_3$  [8] or  $CeO_2$  [9], etc. Especially the  $TiO_2$ , with the physical-chemical stability, unique bandgap structure and photochemical activity, has always been the research hotspot [10–12], since it is first reported in 1972 [13].

For such  $TiO_2$  system, the lower solar utilization and higher photon-generated carrier recombination would always be the most formidable issues [14,15], and a plenty of efficient methods have been attempted in past decades, including the doping, surface modification, heterojunction modification or morphological control. Among these, the doping, with the easy preparation and the universality, has been the preferred way [16], including the metal doping, nonmetal doping or ion doping, such as Shi groups have prepared the C-doped  $TiO_2@g-C_3N_4$  nanoheterojunction for enhancing the photocatalytic  $H_2$  evolution [17], Collins-Martinez groups have reported the Ag doped  $TiO_2$  with

remarkable visible light hydrogen production performance [18], Gao and Yang groups have prepared the N-doped  $TiO_2$  nanobelts as a highly visible-light photocatalyst for hydrogen production [19]. All above would be remarkable results. However, compared with the heterogeneous doping, the  $Ti^{3+}$  self-doping would provide researchers a new method for modifying the  $TiO_2$ , which could improve the visible light absorption, structure matching and stability more efficiently [20,21]. Especially, the  $Ti^{3+}$  could promote to form a self-hydrogenated shell to reduce the activation barrier of the  $H_2$  for enhancing the hydrogen production [22], and series researches have been explored, such as Mao groups have reported the black hydrogenated  $TiO_2$  with increased solar absorption for enhancing the photocatalysis [23], Yu groups have prepared the Cr-SrTiO<sub>3</sub>-modified  $B-TiO_2$  (black  $TiO_2$ ) nanotube arrays for improving the photocatalytic performance [24], Peng groups have fabricated a photoelectrochemical sensor for organic compounds via hydrogenated  $TiO_2$  nanorod arrays [25], etc. Though above praiseworthy results demonstrate researchers a promising fingerpost [26,27], but how to prepare the  $Ti^{3+}$  self-doping  $B-TiO_2$  controllably, economically and steadily are still the most important issue [28], and are studied rarely than other ways. Thus, the preparation of the efficient and stable  $Ti^{3+}$  self-doping  $B-TiO_2$  would be a challenge for the photocatalytic hydrogen production.

On the other hand, the heterojunction modification would be deemed as one of the most efficient ways for ameliorating the high recombination of the photon-generated carrier in photocatalyst. In such

\* Corresponding author.

E-mail address: [crli@zstu.edu.cn](mailto:crli@zstu.edu.cn) (C. Li).

modification, the photon-generated carriers, driven by the heterojunction, would transfer to the lower conduction band (electrons) and higher valence band (holes), which could improve the separation of the photon-generated carriers efficiently [29], and has been achieved by series of works, including the  $\text{Ag}_3\text{PO}_4$  deposition [30],  $\text{Cu}_2\text{O}$  modification [31] or  $\text{ZnS}$ ,  $\text{CdS}$  surface modification [32–34], etc. Especially the  $\text{g-C}_3\text{N}_4$  (graphite phase carbon nitride), with the remarkable visible light response and hydrogen evolution potential, are considered as ideal materials for photocatalytic hydrogen production or surface modification [35], and have been reported as the current hotspot, such as Kang groups have prepared the carbon quantum dots modified  $\text{g-C}_3\text{N}_4$  via water splitting for photocatalytic hydrogen production [36], Safaei groups have fabricated the Z-scheme  $\text{g-C}_3\text{N}_4/\text{BiVO}_4$  photocatalyst for enhancing the photoelectrochemical water splitting [37], Zhang groups have prepared the interlocking  $\text{g-C}_3\text{N}_4/\text{CdS}$  with high efficiency and stable photoelectrochemical hydrogen production [38], Shi groups have prepared the  $\text{Ag}_3\text{PO}_4/\text{g-C}_3\text{N}_4$  composite and obtained a remarkable visible light photocatalytic performance [39]. All above would be regarded as the commendable ways for improving the carrier separation.

What's more, the specific surface area is another important factor for photocatalyst, which could prove sufficient reaction sites for improving the photocatalytic process. There, the morphological control would be the most efficient way to ameliorate this characteristic [40], and a plenty of remarkable morphologies have been reported, such as nanoparticles, nanowires, nanotubes or nanosheets [41,42]. Herein, the hollow nanosphere would be a commendable choice, because that the hollow structure could remain multiple reflections for increasing the visible light absorption and the inside-outside walls could provide double specific surface areas for increasing the reaction sites [43], similar researches have been reported in previous literatures, such as Lan groups have prepared the hollow  $\text{ZnO}$  nanospheres for improving the photocatalytic performance [44], Biswas groups have reported the  $\text{ZnO}_{1-x}$ /carbondots composite hollow spheres as a remarkable photocatalyst [45], Wang groups have fabricated the hollow  $\text{Bi}_2\text{WO}_6$  for enhancing photocatalytic  $\text{CO}_2$  photoreduction [46], and so on. Thus, the hollow core-shell nanospheres would be identified as a preferential method for regulating the nano-heterojunction.

In this work, we synthesized the  $\text{Ti}^{3+}$  self-doping  $\text{B-TiO}_2/\text{g-C}_3\text{N}_4$  hollow core-shell nano-heterojunction by continuous two-step hydrothermal deposition and sculpture-reduction processes. Compared with the normal  $\text{TiO}_2$  or  $\text{g-C}_3\text{N}_4$ , the  $\text{B-TiO}_2/\text{g-C}_3\text{N}_4$  nano-heterojunction exhibits an obvious enhancement in photocatalytic hydrogen production (about 18 fold of the normal  $\text{TiO}_2$  and 65 fold of the  $\text{g-C}_3\text{N}_4$ ). Further, the mechanism of the photocatalytic hydrogen production enhancement is studied by the continuous electrochemical testing.

## 2. Experimental

The  $\text{Ti}^{3+}$  self-doping  $\text{B-TiO}_2/\text{g-C}_3\text{N}_4$  hollow core-shell nano-heterojunction were prepared via the template method of the depositing with the  $\text{TiO}_2$  and  $\text{g-C}_3\text{N}_4$  continuously, then sculpturing and reducing by the  $\text{NH}_4\text{HF}_2$  (4 mol/L, 12 h) and  $\text{NaBH}_4$  (0.5 g, 30 min). The schematic diagram is shown in Fig. 1 and the details are displayed in ESI,

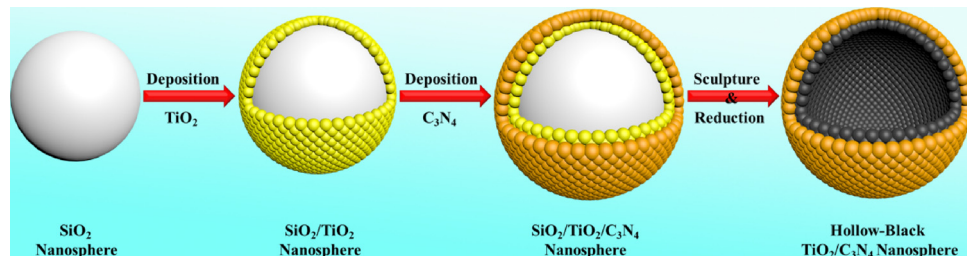


Fig. 1. The schematic diagram of the preparation of the  $\text{Ti}^{3+}$  self-doping  $\text{B-TiO}_2/\text{g-C}_3\text{N}_4$  hollow core-shell nano-heterojunction.

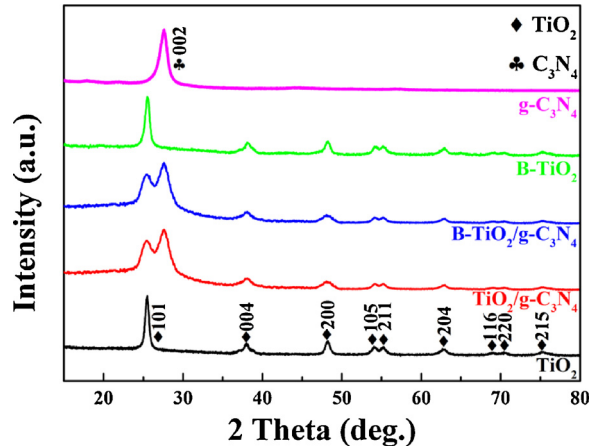


Fig. 2. The XRD of the samples.

including the characterization and photocatalytic activity.

## 3. Results and discuss

Fig. 2 is the XRD spectra of the samples, including the normal  $\text{TiO}_2$ ,  $\text{B-TiO}_2$ ,  $\text{TiO}_2/\text{g-C}_3\text{N}_4$ ,  $\text{B-TiO}_2/\text{g-C}_3\text{N}_4$  and  $\text{g-C}_3\text{N}_4$ . As revealed, the diffraction peaks at 25.5, 38.0, 48.2, 54.0, 55.2, 62.9, 68.9, 70.4 and 75.2° could be ascribed to the (101), (004), (200), (105), (211), (204), (116), (220) and (215) planes of the  $\text{TiO}_2$  (PDF#21-1272) [26,27]. With the deposition of the  $\text{g-C}_3\text{N}_4$ , the obvious new diffraction peak locates at 27.6° is attributed to the (002) plane of the layer stacking of conjugated aromatic rings on  $\text{g-C}_3\text{N}_4$  (PDF#87-1526) [29]. It's interesting that, with the reduction, the diffraction peaks of the  $\text{B-TiO}_2$  change hardly, including the  $\text{B-TiO}_2$  and  $\text{B-TiO}_2/\text{g-C}_3\text{N}_4$ , which indicate that the structure of the  $\text{TiO}_2$  is stable and is benefit for the continuous photocatalysis. There is no other diffraction peak could be observed, which imply that the core-shell nano-heterojunction is composed of  $\text{TiO}_2$  and  $\text{g-C}_3\text{N}_4$ .

Fig. 3 is the SEM of the samples. As shown in Fig. 3a, the as-prepared  $\text{SiO}_2$  nanospheres with diameter of about 400 nm are smooth and uniform. Then, with the deposition of the  $\text{TiO}_2$  (Fig. 3b) and  $\text{g-C}_3\text{N}_4$  (Fig. 3c), the surfaces of the samples turn to be rough. Further, with the sculpture and reduction, the hollow core-shell nano-heterojunction has formed and could be observed clearly in Fig. 3d. It's interesting that, in the sculpture-reduction process, the samples could maintain the sphere, which is benefit for forming the hollow core-shell structure. Further, the elemental mappings of the  $\text{B-TiO}_2/\text{g-C}_3\text{N}_4$  nano-heterojunctions are shown in Fig. S1 (ESI). As revealed, the elements of Ti, N and C are distributed on the surface uniformly, which corresponds to the hollow core-shell structure.

In addition, the specific surface area of the  $\text{B-TiO}_2/\text{g-C}_3\text{N}_4$  nano-heterojunctions is calculated by the Brunauer–Emmett–Teller (BET) equation through  $\text{N}_2$  adsorption–desorption isotherm measurement [47]. As displayed in Fig. S2a (in ESI), the  $\text{B-TiO}_2/\text{g-C}_3\text{N}_4$  nano-heterojunction, with a specific surface area of 96.80  $\text{m}^2/\text{g}$ , is a typical

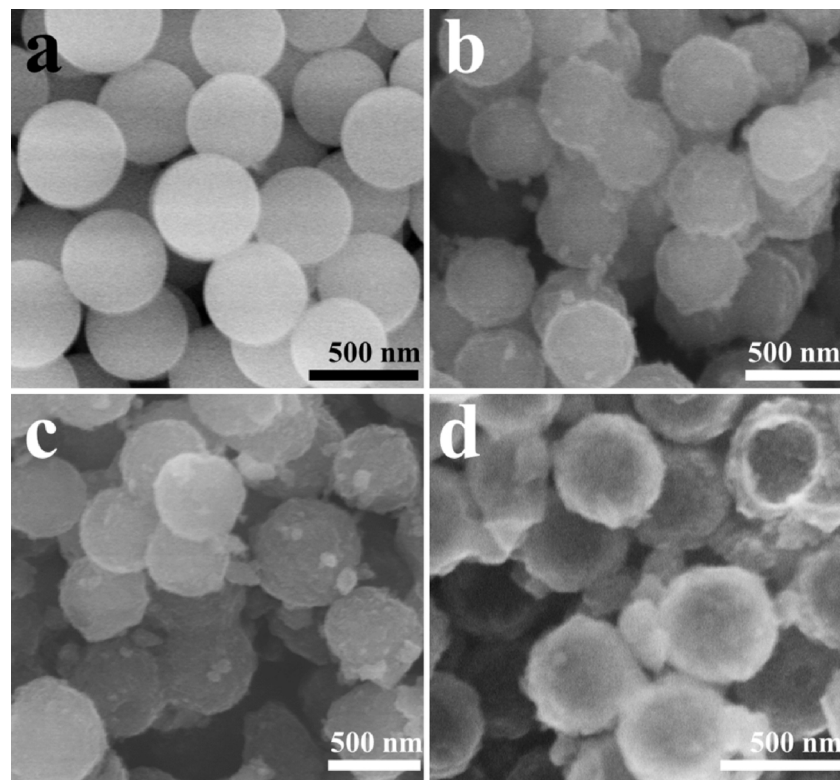


**Fig. 3.** The SEM of the samples, (a)  $\text{SiO}_2$  nanospheres, (b)  $\text{SiO}_2/\text{TiO}_2$  nanospheres, (c) the  $\text{SiO}_2/\text{TiO}_2/\text{g-C}_3\text{N}_4$  nanospheres, (d)  $\text{B-TiO}_2/\text{g-C}_3\text{N}_4$  hollow nano-heterojunction.

hollow core-shell structure. Further, calculated by the Barrett–Joyner–Halenda (BJH) equation, the average size of the pores is about 10.24 nm (in ESI Fig. S2b). All above characteristics are beneficial for improving the photocatalytic performance.

Fig. 4 is the TEM of the as-prepared  $\text{B-TiO}_2/\text{g-C}_3\text{N}_4$  nano-heterojunctions. As displayed in Fig. 4a, the nano-heterojunction with diameter of about 400 nm exhibit obvious hollow core-shell structure. Fig. 4b is the interface of the  $\text{B-TiO}_2/\text{g-C}_3\text{N}_4$ , as shown, the  $\text{g-C}_3\text{N}_4$  shell covers on the surface of the hollow  $\text{TiO}_2$  nanosphere, which corresponds to the SEM and is regarded as an important advantage for photocatalysis. Further, the HRTEM of the  $\text{B-TiO}_2$  and  $\text{g-C}_3\text{N}_4$  are shown in Fig. 4c and d, the lattice spaces of 0.350 nm and 0.327 nm are ascribed to the (101) plane of the  $\text{TiO}_2$  and (002) plane of the  $\text{g-C}_3\text{N}_4$  [26, 29,], respectively.

$\text{C}_3\text{N}_4$  [26, 29,], respectively.

Furthermore, the XPS spectra are performed to illuminate the components and chemical states of the as-prepared  $\text{Ti}^{3+}$  self-doping  $\text{B-TiO}_2/\text{g-C}_3\text{N}_4$  nano-heterojunction. Fig. 5a presents the full survey, which indicates the presence of Ti, O, C and N in the  $\text{B-TiO}_2/\text{g-C}_3\text{N}_4$  nano-heterojunction. Fig. 5b illuminates the high-resolution spectra of the Ti 2p. As revealed, the two main peaks of  $\text{Ti} 2p_{3/2}$  and  $\text{Ti} 2p_{1/2}$  could be fitted into four peaks, that the peaks of 457.7 and 463.6 eV are attributed to the  $\text{Ti}^{3+} 2p_{3/2}$  and  $\text{Ti}^{3+} 2p_{1/2}$ , the peaks of 458.6 and 464.8 eV are attributed to the  $\text{Ti}^{4+} 2p_{3/2}$  and  $\text{Ti}^{4+} 2p_{1/2}$ , respectively, which indicate that the  $\text{Ti}^{3+}$  has formed in the reduction process [27, 28]. Further, the O 1s, revealed in Fig. 5c, could be divided into three peaks of 529.7, 530.6 and 532.2 eV, which could be ascribed to

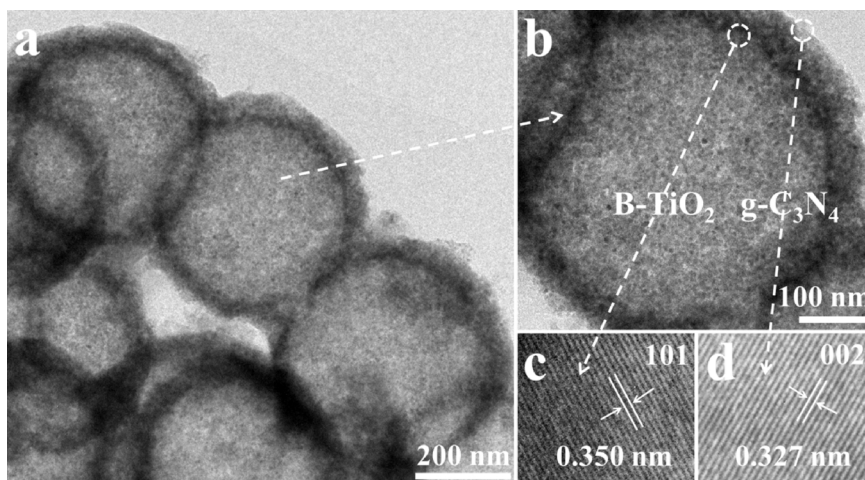


**Fig. 4.** The TEM of the as-prepared nano-heterojunction, (a) the TEM of the  $\text{B-TiO}_2/\text{g-C}_3\text{N}_4$ , (b) the interface of the  $\text{B-TiO}_2/\text{g-C}_3\text{N}_4$ , (c) the HRTEM of the  $\text{B-TiO}_2$  (d) the HRTEM of the  $\text{g-C}_3\text{N}_4$ .

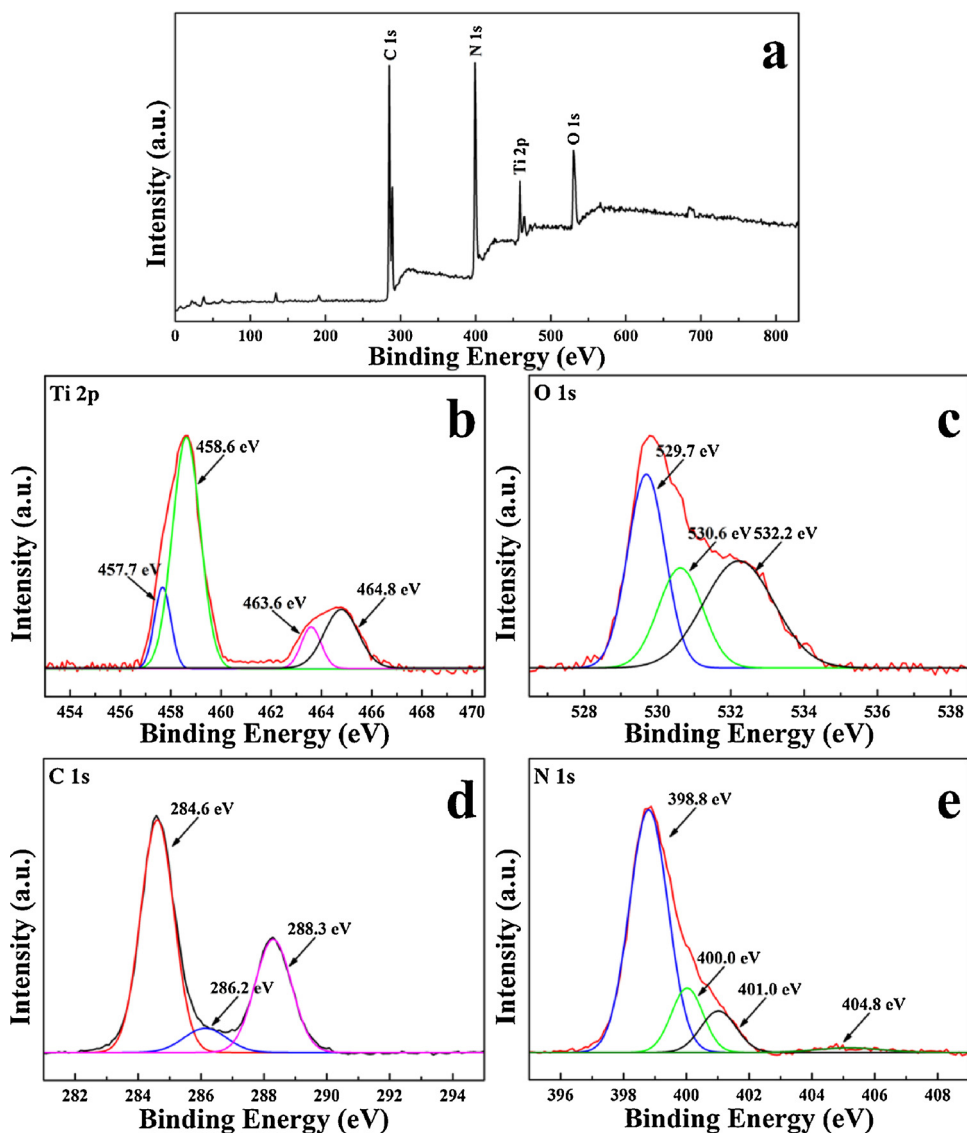


Fig. 5. The XPS of the B-TiO<sub>2</sub>/g-C<sub>3</sub>N<sub>4</sub> nano-heterojunction, (a) full survey, (b) Ti 2p spectra, (c) O 1s spectra, (d) C 1s spectra, (e) N 1s spectra.

the Ti–O bond in structure, the –OH bond adsorbed on the surface [28,29], and the oxygen vacancy(O<sub>v</sub>) in the vicinity of Ti<sup>3+</sup> [22,28], respectively, that could be considered as a convincingly evidence of the presence of Ti<sup>3+</sup>. Fig. 5d and e are high-resolution XPS spectra of the C 1s and N 1s. As revealed in Fig. 5d, fitted by the Gaussian analysis method, the peaks of C 1s could be divided to three distinct peaks at 284.6, 286.2 and 288.3 eV, which could be attributed to the sp<sup>2</sup> C–C bonds, the C–NH<sub>2</sub> species of the g-C<sub>3</sub>N<sub>4</sub> [28,44], and the carbon in N–C=N [29,48], respectively. As illustrated in Fig. 5e, the high resolution N 1s spectrum could be deconvoluted into four characteristic peaks. There, the peak at 398.8 and 400.0 are attributed to the sp<sup>2</sup> hybridized nitrogen in the triazine rings (C–N=C) and the tertiary nitrogen N–(C)<sub>3</sub> groups [29,48] together with the N–C=N (288.3 eV), respectively. What's more, the peaks locate at 401.0 and 404.8 eV correspond to the free amino groups (C–N–H) and π-excitations [48], respectively.

Furthermore, the FT-IR spectra of the different samples are displayed in Fig. 6. As revealed, there's no obvious characteristic peak could be observed in normal TiO<sub>2</sub>, except the 1637 cm<sup>-1</sup> [28], which could also be observed in all of the samples and ascribed to the hydroxyl group and physically absorbed water on the surface. With the deposition of the g-C<sub>3</sub>N<sub>4</sub>, five new distinct characteristic peaks could be

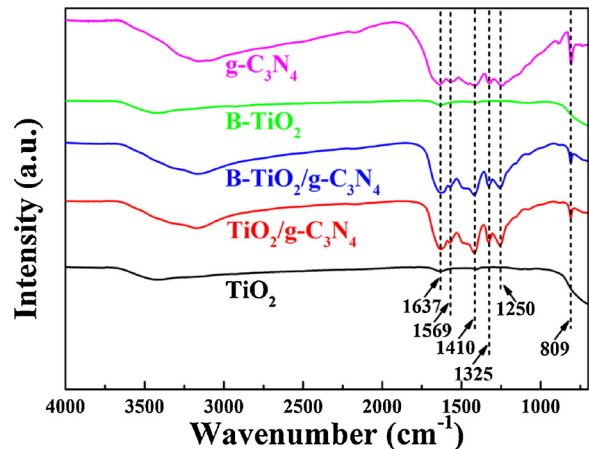


Fig. 6. The FT-IR spectra of the TiO<sub>2</sub>, TiO<sub>2</sub>/g-C<sub>3</sub>N<sub>4</sub>, B-TiO<sub>2</sub>/g-C<sub>3</sub>N<sub>4</sub>, B-TiO<sub>2</sub> and g-C<sub>3</sub>N<sub>4</sub>.

observed, the peaks at 1250, 1325, 1410 and 1569 cm<sup>-1</sup> could be attributed to the aromatic C–N stretching vibration modes, and the peak at 809 cm<sup>-1</sup> is ascribed to the triazine units [27–29], that correspond to

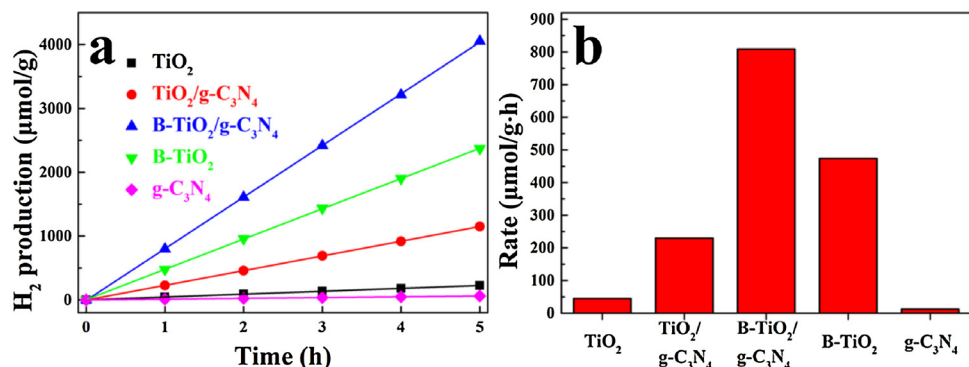


Fig. 7. Photocatalytic hydrogen production activity, (a) the photocatalytic activity of different samples, (b) the histograms of the different samples.

the pure g-C<sub>3</sub>N<sub>4</sub> and indicates the modification could affect the structure of g-C<sub>3</sub>N<sub>4</sub> hardly. It's interesting that, with the sculpture-reduction process, there is no other new characteristic peak could be observed, which manifest that the sculpture-reduction process hasn't introduced other surface groups, and correspond to the results of XPS.

Thus, the Ti<sup>3+</sup> self-doping B-TiO<sub>2</sub>/g-C<sub>3</sub>N<sub>4</sub> hollow core-shell nano-heterojunction has been fabricated successfully.

The photocatalytic hydrogen production performance of the different samples is revealed in Fig. 7, including the TiO<sub>2</sub>, TiO<sub>2</sub>/g-C<sub>3</sub>N<sub>4</sub>, B-TiO<sub>2</sub>/g-C<sub>3</sub>N<sub>4</sub>, B-TiO<sub>2</sub> and g-C<sub>3</sub>N<sub>4</sub>. As revealed, the normal TiO<sub>2</sub> nanospheres exhibit weaker H<sub>2</sub> production of ~45.04 μmol/g·h, which could be ascribed to the intrinsic H<sub>2</sub> production performance of the TiO<sub>2</sub>. It's evident that, with introducing of the g-C<sub>3</sub>N<sub>4</sub> and the sculpture-reduction process, the hydrogen production performance exhibits an obvious enhancement and gets an optimal value at the B-TiO<sub>2</sub>/g-C<sub>3</sub>N<sub>4</sub> (~808.97 μmol/g·h). By calculating, the hydrogen production performance of the B-TiO<sub>2</sub>/g-C<sub>3</sub>N<sub>4</sub> hollow core-shell nano-heterojunction is about 18 times than the normal TiO<sub>2</sub> nanospheres, which indicates that the B-TiO<sub>2</sub> and heterojunction would be the main factors for the photocatalytic hydrogen production enhancement. As a control group, the as-prepared B-TiO<sub>2</sub> and g-C<sub>3</sub>N<sub>4</sub> are also carried out at the same condition. As displayed, there are about ~474.34 and ~12.37 μmol/g·h H<sub>2</sub> produce from the B-TiO<sub>2</sub> and g-C<sub>3</sub>N<sub>4</sub> respectively, which would be valid evidences for that the nano-heterojunction could enhance the photocatalytic hydrogen production efficiently.

Based on the remarkable photocatalytic hydrogen production performance, it's significant to explore the cycling stability of the as-prepared B-TiO<sub>2</sub>/g-C<sub>3</sub>N<sub>4</sub> hollow core-shell nano-heterojunction. As shown in Fig. 8, in 30 h (6 consecutive cycles) hydrogen production process, the B-TiO<sub>2</sub>/g-C<sub>3</sub>N<sub>4</sub> nano-heterojunction exhibits a commendable stability and obtains a higher average of about 794.90 μmol/g·h, that closes to the initial value (808.97 μmol/g·h) and could be deemed as a comforting result. As shown in Fig. S3 (ESI), the XRD of the sample after reaction exhibits similar diffraction peaks as the initial sample, which

indicates that the as-prepared B-TiO<sub>2</sub>/g-C<sub>3</sub>N<sub>4</sub> nano-heterojunction obtains a prominent stability in the photocatalytic process.

All above results manifest that the sculpture-reduction process and nano-heterojunction could improve the photocatalytic hydrogen production performance and cycling stability efficiently. Thus, exploring the mechanism of the B-TiO<sub>2</sub>/g-C<sub>3</sub>N<sub>4</sub> nano-heterojunction in the photocatalytic hydrogen production process would be a significant issue.

Fig. 9 shows the UV-vis absorption spectra of the different samples. As revealed, the obviously absorption locates at approximately 380 nm could be ascribed to the intrinsic band gap of the normal TiO<sub>2</sub> [24–26]. With the introducing of g-C<sub>3</sub>N<sub>4</sub>, the absorption of the nano-heterojunction exhibits an obviously red-shift in visible light, which could be attributed to the absorption of the g-C<sub>3</sub>N<sub>4</sub> and corresponds to the intrinsic absorption of the pure g-C<sub>3</sub>N<sub>4</sub> [28,29]. Subsequently, with the sculpture-reduction process, the B-TiO<sub>2</sub>/g-C<sub>3</sub>N<sub>4</sub> nano-heterojunction exhibits an evident absorption in visible light, which is attributed to the Ti<sup>3+</sup> and the O<sub>v</sub>, and corresponds to the absorption of the pure B-TiO<sub>2</sub> [22,25,27,28]. It's obvious that the increasing absorption would be regarded as an important reason for the photocatalytic hydrogen production enhancement. It's interesting that the pure B-TiO<sub>2</sub> nanospheres exhibit stronger visible light absorption than the B-TiO<sub>2</sub>/g-C<sub>3</sub>N<sub>4</sub>, while the optimal hydrogen production performance is obtained at the B-TiO<sub>2</sub>/g-C<sub>3</sub>N<sub>4</sub>, which indicates that the nano-heterojunction at the interface would also play an important role in the photocatalytic hydrogen production.

In this core-shell nano-heterojunction, the separation and transfer of the photon-generated carriers would be important factors for the photocatalytic performance, and the transient photocurrent response and EIS (electrochemical impedance spectroscopy) Nyquist plots of the TiO<sub>2</sub>, TiO<sub>2</sub>/g-C<sub>3</sub>N<sub>4</sub>, B-TiO<sub>2</sub>/g-C<sub>3</sub>N<sub>4</sub>, B-TiO<sub>2</sub> and g-C<sub>3</sub>N<sub>4</sub> are revealed in Fig. 10. As revealed in Fig. 10a, with the deposition and sculpture-reduction process, the transient photocurrents of the samples exhibit an obvious enhancement under the continuously illumination switch on and off. By calculating, the transient photocurrents of each sample are

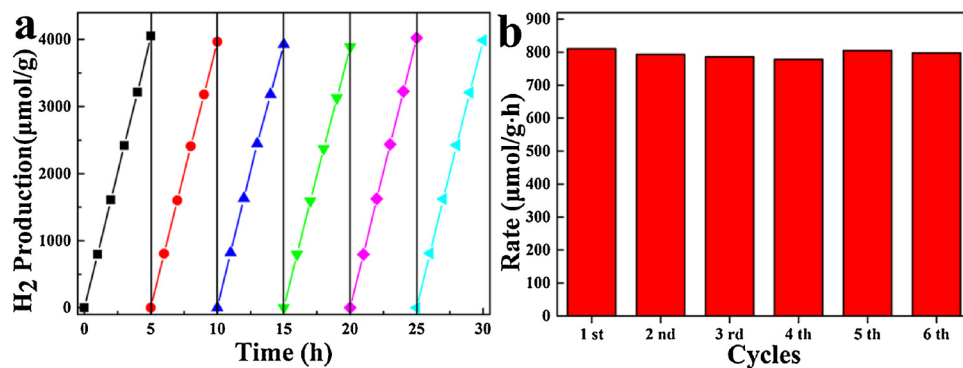


Fig. 8. (a) The cycle curve of the B-TiO<sub>2</sub>/g-C<sub>3</sub>N<sub>4</sub> hollow core-shell nano-heterojunction, (b) the histogram of the samples.

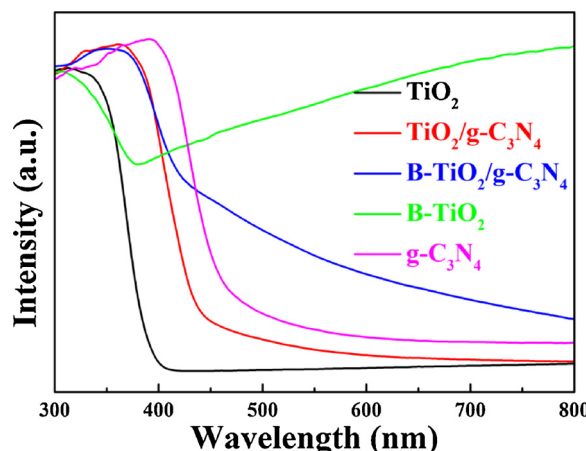


Fig. 9. The UV-vis absorption spectra of the  $\text{TiO}_2$ ,  $\text{TiO}_2/\text{g-C}_3\text{N}_4$ ,  $\text{B-TiO}_2/\text{g-C}_3\text{N}_4$ ,  $\text{B-TiO}_2$  and  $\text{g-C}_3\text{N}_4$ .

$3.4 \times 10^{-2}$  ( $\text{TiO}_2$ ),  $6.4 \times 10^{-2}$  ( $\text{TiO}_2/\text{g-C}_3\text{N}_4$ ),  $24.1 \times 10^{-2}$  ( $\text{B-TiO}_2/\text{g-C}_3\text{N}_4$ ),  $12.3 \times 10^{-2}$  ( $\text{B-TiO}_2$ ) and  $1.8 \times 10^{-2}$  ( $\text{g-C}_3\text{N}_4$ )  $\mu\text{A}$ , respectively. There, the increased photocurrent could be majorly ascribed to the efficient photo-generated separation and transferring, which is benefit for the photocatalysis and correspond to the results of photocatalytic performance [27,28,49]. Further, as demonstrated in Fig. 10b, the EIS Nyquist plots are deemed as another valid methods to investigate the migration and interface transfer/recombination rates of charge carriers [27,28,49]. As shown, the radius of the circular arc decreases with the deposition of the  $\text{g-C}_3\text{N}_4$  and sculpture-reduction process, and obtains the smallest value at  $\text{B-TiO}_2/\text{g-C}_3\text{N}_4$ , which indicate the  $\text{B-TiO}_2/\text{g-C}_3\text{N}_4$  obtains more effective separation of photo-generated carriers and higher efficiency of charge immigration across the heterojunction interface, that corresponds to the results of the transient photocurrent response. In addition, the PL is regarded as another important information to evaluate the separation of the photo-generated carriers [29]. As revealed in the Fig. S4 (ESI), the sample of  $\text{B-TiO}_2/\text{g-C}_3\text{N}_4$  exhibits the lower PL than the  $\text{g-C}_3\text{N}_4$  and  $\text{TiO}_2/\text{g-C}_3\text{N}_4$ , which indicate that the heterojunction modification and sculpture-reduction process could decrease the recombination of the photo-generated carriers efficiently and corresponds to the above results. From these above, including the transient photocurrent response, EIS Nyquist plots and PL, the  $\text{B-TiO}_2/\text{g-C}_3\text{N}_4$  nano-heterojunction, with high photo-generated carrier separation and faster charge transfer, could increase the lifetime of the photo-generated carrier to improving the photocatalytic hydrogen production activity.

Moreover, the type of semiconductor and band potential of the  $\text{g-C}_3\text{N}_4$  and  $\text{B-TiO}_2$  are the basic factors for designing this nano-heterojunction. Thus, the electrochemical Mott-Schottky experiment is performed. There, based on the Mott-Schottky equation, the capacitance

(C) depend on applied potential could be fitted as follows [50,51]:

$$\frac{1}{C^2} = \pm \frac{2}{e\epsilon\epsilon_0 N_d} \left( E - E_{FB} - \frac{K_b T}{e} \right)$$

where, the slope denotes the type of semiconductor (positive to n-type and negative to p-type) and the  $N_d$  denotes the carrier density. Further, the C, E (corrected by the AgCl vs 0.197 eV) and the intercept on the x-axis denote the space charge capacitance, applied potential and  $E_{FB}$  (band potential), respectively. As revealed in Fig. 11, the positive slope in the Mott-Schottky plot indicates that both of the  $\text{g-C}_3\text{N}_4$  and  $\text{B-TiO}_2$  are typical n-type semiconductors [51,52]. Furthermore, by calculating, the flat band potential of the  $\text{g-C}_3\text{N}_4$  and  $\text{B-TiO}_2$  are  $-0.95$  (vs AgCl) and  $-0.66$  eV (vs AgCl), respectively. Combined with the band gap of each other and corrected by the AgCl, the CB (conduction band) of  $\text{g-C}_3\text{N}_4$  and  $\text{TiO}_2$  could be calculated to be  $-0.75$  eV (vs NHE) and  $-0.46$  eV (vs NHE), and the valence band locate at  $1.85$  eV (vs NHE) and  $1.98$  eV (vs NHE), respectively. Compared with the Fig. S5 (ESI), the CB of the  $\text{B-TiO}_2$  is more negative than the normal  $\text{TiO}_2$ , which is more benefit for the HER (hydrogen evolution reaction) and is an advantage of this  $\text{B-TiO}_2$ . Hence, it's obvious that the photon-generated electrons would transfer to the CB of  $\text{TiO}_2$  and the photon-generated holes would transfer to the VB of  $\text{g-C}_3\text{N}_4$  [27–29], which could promote the separation of the photon-generated carriers efficiently and is regarded as the unique advantage for this core-shell heterojunction structure.

Based on the above results, including the morphology, structure and electrochemistry test, the mechanism of the photocatalytic hydrogen production enhancement of the  $\text{Ti}^{3+}$  self-doping  $\text{B-TiO}_2/\text{g-C}_3\text{N}_4$  hollow core-shell nano-heterojunction could be proposed as the Fig. 12, which could be ascribed to the  $\text{Ti}^{3+}$  and  $\text{O}_v$  in the  $\text{B-TiO}_2$ , interface nano-heterojunction and the hollow core-shell structure.

As revealed in Figs. 7 and 9, the  $\text{B-TiO}_2/\text{g-C}_3\text{N}_4$  and  $\text{B-TiO}_2$ , with stronger visible light absorption, exhibit much preferable photocatalytic hydrogen production than that of normal  $\text{TiO}_2$ ,  $\text{g-C}_3\text{N}_4$  or  $\text{TiO}_2/\text{g-C}_3\text{N}_4$ , which could be ascribed to the unique donor level of the  $\text{O}_v$  (O vacancy) and  $\text{Ti}^{3+}$  in the  $\text{B-TiO}_2$  [21,24]. There, the  $\text{O}_v$  could form a new sublevel state at the bottom of the  $\text{TiO}_2$  conduction band, which could increase the visible light absorption and speed up the photo-generated charge carrier separation for improving the visible light response [26–28], and is considered as an important reason for photocatalysis. Further, in the presence of adsorbed water, induced by the  $\text{Ti}^{3+}$ , the hydrogen atoms would diffuse into the  $\text{TiO}_2$  to form a self-hydrogenated shell on the interface [22], which could reduce the activation barrier of the  $\text{H}_2$ , make the water protons to photo-excited stage and promote the hydrogen diffusing to the subsurface more easily for enhancing the hydrogen production [22,27,28,53,54], that is considered as one of the most important reasons for hydrogen production enhancement and has been proved by current researches [22]. In addition, the more negative CB of the  $\text{B-TiO}_2$  would be one more advantage for HER. It's interesting that though the pure  $\text{B-TiO}_2$

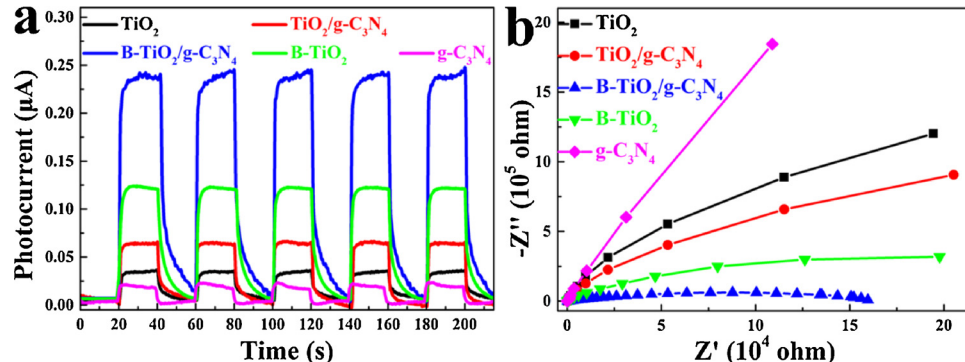
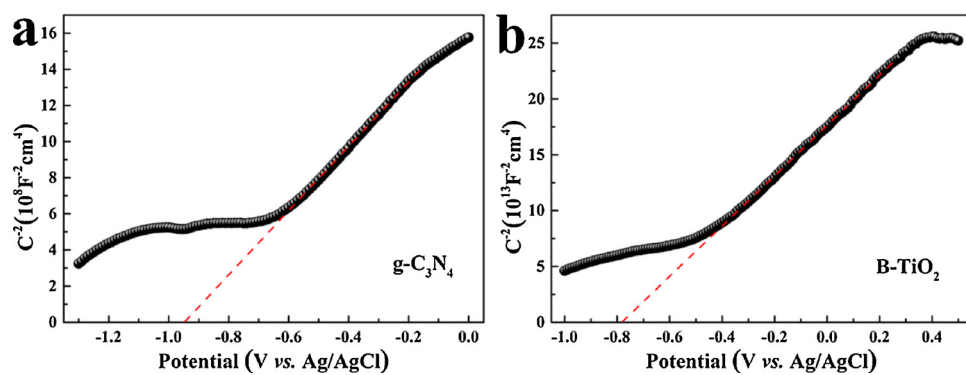
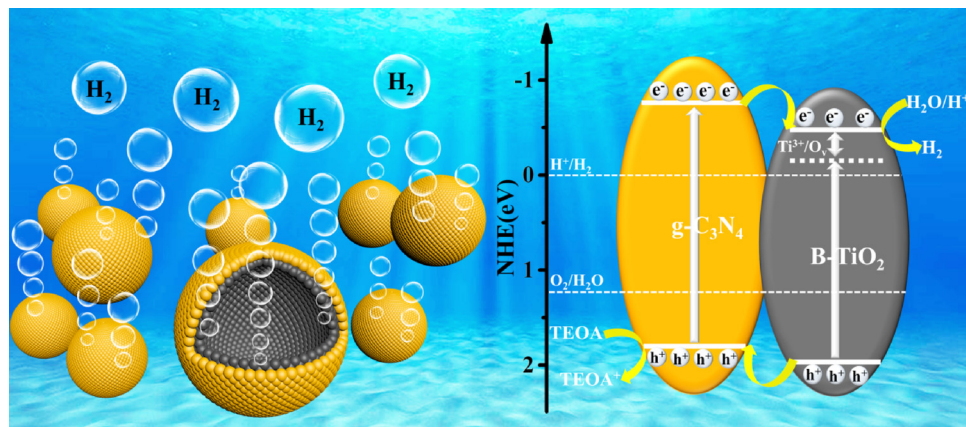


Fig. 10. (a) Transient photocurrent response and (b) EIS Nyquist plots of the  $\text{TiO}_2$ ,  $\text{TiO}_2/\text{g-C}_3\text{N}_4$ ,  $\text{B-TiO}_2/\text{g-C}_3\text{N}_4$ ,  $\text{B-TiO}_2$  and  $\text{g-C}_3\text{N}_4$ .

Fig. 11. The Mott-Schottky plots of the samples, (a)  $\text{g-C}_3\text{N}_4$ , (b)  $\text{B-TiO}_2$ .Fig. 12. The photocatalytic hydrogen production mechanism of the  $\text{Ti}^{3+}$  self-doping  $\text{B-TiO}_2/\text{g-C}_3\text{N}_4$  hollow core-shell nano-heterojunction.

nanospheres obtain more intense absorption in visible light, but the  $\text{B-TiO}_2/\text{g-C}_3\text{N}_4$  heterojunction exhibits more excellent photocatalytic hydrogen production (similar as the  $\text{TiO}_2/\text{g-C}_3\text{N}_4$  and pure  $\text{g-C}_3\text{N}_4$ ), which indicates that the nano-heterojunction would be another important reason for the enhancement. In such system, under illumination, driven by the internal electric field of the nano-heterojunction, the excited photon-generated electron (CB of  $\text{g-C}_3\text{N}_4$ ) would transfer to the  $\text{B-TiO}_2$  (CB of  $\text{B-TiO}_2$ ) and the photon-generated holes (VB of  $\text{B-TiO}_2$ ) would transfer to the  $\text{g-C}_3\text{N}_4$  (VB of  $\text{g-C}_3\text{N}_4$ ), which could provide a more efficient charge carriers separation for increasing the lifetime of the photon-generated carriers [28,29]. Incorporated with the induction of  $\text{O}_v$  and  $\text{Ti}^{3+}$ , the long lifetime photon-generated electrons could reducing the  $\text{H}^+$  much more efficiently to enhance the photocatalytic hydrogen production [22,28]. This process could be proved by the results of TEM, transient photocurrent, PL, EIS and Mott-Schottky plots, and is deemed as the most believable explanation for the enhanced photocatalytic hydrogen production.

Additionally, the hollow core-shell structure also plays a prominent role, because that the double walls could provide large specific surface areas ( $\text{B-TiO}_2/\text{g-C}_3\text{N}_4$ ,  $96.80 \text{ m}^2/\text{g}$ ) for the photocatalytic hydrogen production [43] and the hollow nanospheres could remain multiple reflections for increasing visible light utilization.

Thus, the  $\text{Ti}^{3+}$  self-doping  $\text{B-TiO}_2/\text{g-C}_3\text{N}_4$  hollow core-shell nano-heterojunction exhibits obvious enhancement of photocatalytic hydrogen production performance under illumination.

#### 4. Conclusions

We have successfully prepared the  $\text{Ti}^{3+}$  self-doping  $\text{B-TiO}_2/\text{g-C}_3\text{N}_4$  hollow core-shell nano-heterojunction via simple hydrothermal deposition and sculpture-reduction processes. The as-prepared  $\text{B-TiO}_2/\text{g-C}_3\text{N}_4$  hollow core-shell nano-heterojunction exhibits remarkable

photocatalytic enhancement towards the hydrogen production, with a catalytic activity nearly 18 times and 65 times than that of normal  $\text{TiO}_2$  and  $\text{g-C}_3\text{N}_4$ , respectively. There, the  $\text{O}_v$ ,  $\text{Ti}^{3+}$  self-doping and core-shell nano-heterojunction would be regarded as the main reasons, in which the  $\text{O}_v$  could improve the visible light response,  $\text{Ti}^{3+}$  could induced the interface to form a self-hydrogenated shell for reducing the activation barrier of the  $\text{H}_2$ , and the core-shell heterojunction could drive the transfer of photon-generated carriers to promote the photon-generated carrier separation, those could reducing the  $\text{H}^+$  efficiently to enhance the photocatalytic hydrogen production. What's more, the abundant specific surface areas of the hollow core-shell nanospheres would be another reason. Additionally, the photocatalyst exhibits remarkable photocatalytic stability in continuous photocatalysis.

Thus, the design of the  $\text{Ti}^{3+}$  self-doping  $\text{B-TiO}_2/\text{g-C}_3\text{N}_4$  hollow core-shell nano-heterojunction would provide a new sight for designing the potential hydrogen production materials.

#### Acknowledgments

This work was supported by the Natural Science Foundation of China (Nos. 51672249, 51603187 and 11747136) and the Zhejiang Provincial Natural Science Foundation of China (No. LQ17F040004).

#### Appendix A. Supplementary data

Supplementary material related to this article can be found, in the online version, at doi:<https://doi.org/10.1016/j.apcatb.2018.09.079>.

#### References

- [1] M. Zhou, Q.H. Weng, Z.I. Popov, Y.J. Yang, L.Y. Antipina, P.B. Sorokin, X. Wang, Y. Bando, D. Golberg, Construction of polarized carbon-nickel catalytic surfaces for

potent, durable, and economic hydrogen evolution reactions, *ACS Nano* 12 (2018) 4148–4155.

[2] K. Zhang, G. Zhang, J.H. Qu, H.J. Liu, Intensification of anodic charge transfer by contaminant degradation for efficient H<sub>2</sub> production, *J. Mater. Chem. A Mater. Energy Sustain.* 6 (2018) 10297–10303.

[3] S.Q. Qu, W. Chen, J.S. Yu, G.L. Chen, R. Zhang, S.J. Chu, J. Huang, X.Q. Wang, C.R. Li, K. Ostrikov, Cross-linked trimetallic nanopetals for electrocatalytic water splitting, *J. Power Sources* 390 (2018) 224–233.

[4] C. Zhang, Y.M. Zhou, J.H. Bao, X.L. Sheng, J.S. Fang, S. Zhao, Y.W. Zhang, W.X. Chen, Hierarchical honeycomb Br<sup>-</sup>, N-codoped TiO<sub>2</sub> with enhanced visible-light photocatalytic H<sub>2</sub> production, *ACS Appl. Mater. Interface* 10 (2018) 18796–18804.

[5] Y. Liu, S.P. Ding, Y.Q. Shi, X.F. Liu, Z.Z. Wu, Q.Q. Jiang, T.F. Zhou, N.K. Liu, J.C. Hu, Construction of CdS/CoO<sub>x</sub> core-shell nanorods for efficient photocatalytic H<sub>2</sub> evolution, *Appl. Catal. B Environ.* 234 (2018) 109–116.

[6] S.J. Liang, B. Han, X.M. Liu, W.Y. Chen, M. Peng, G.J. Guan, H. Deng, Z. Lin, 3D spatially branched hierarchical Z-scheme CdS-Au nanoclusters-ZnO hybrids with boosted photocatalytic hydrogen evolution, *J. Alloys Compd.* 754 (2018) 105–113.

[7] J. Li, Y. Peng, X.H. Qian, J. Lin, Few-layer Co-doped MoS<sub>2</sub> nanosheets with rich active sites as an efficient catalyst for photocatalytic H<sub>2</sub> production over CdS, *Appl. Surf. Sci.* 452 (2018) 437–442.

[8] H.D. Chen, F. Zhang, X.W. Sun, W.F. Zhang, G.Q. Li, Effect of reaction atmosphere on photodeposition of Pt nanoparticles and photocatalytic hydrogen evolution from SrTiO<sub>3</sub> suspension system, *Int. J. Hydrogen Energy* 43 (2018) 5331–5336.

[9] P. Zhang, Y. Liu, B.Z. Tian, Y.S. Luo, J.L. Zhang, Synthesis of core-shell structured CdS@CeO<sub>2</sub> and CdS@TiO<sub>2</sub> composites and comparison of their photocatalytic activities for the selective oxidation of benzyl alcohol to benzaldehyde, *Catal. Today* 281 (2017) 181–188.

[10] G. Halasi, A. Toth, T. Bansagi, F. Solymosi, Production of H<sub>2</sub> in the photocatalytic reactions of ethane on TiO<sub>2</sub>-supported noble metals, *Int. J. Hydrogen Energy* 41 (2016) 13485–13492.

[11] G. Yang, H. Ding, D.M. Chen, J.J. Feng, Q. Hao, Y.F. Zhu, Construction of urchin-like ZnIn<sub>2</sub>S<sub>4</sub>-Au-TiO<sub>2</sub> heterostructure with enhanced activity for photocatalytic hydrogen evolution, *Appl. Catal. B Environ.* 234 (2018) 260–267.

[12] Q. Quan, S.J. Xie, B. Weng, Y. Wang, Y.J. Xu, Revealing the double-edged sword role of graphene on boosted charge transfer versus active site control in TiO<sub>2</sub> nanotube arrays@RGO/MoS<sub>2</sub> heterostructure, *Small* 14 (2018) 1704531.

[13] A. Fujishima, K. Honda, Electrochemical photolysis of water at a semiconductor electrode, *Nature* 238 (1972) 37–38.

[14] D.W. Ding, K. Liu, S.N. He, C.B. Gao, Y.D. Yin, ligand-exchange assisted formation of Au/TiO<sub>2</sub>schottky contact for visible-light photocatalysis, *Nano Lett.* 14 (2014) 6731–6736.

[15] Y.Q. Yang, G. Liu, J.T.S. Irvine, H.M. Cheng, Enhanced photocatalytic H<sub>2</sub> production in core-shell engineered rutile TiO<sub>2</sub>, *Adv. Mater.* 28 (2016) 5850–5856.

[16] D.N. Li, Y. Chen, F. Yin, L.Z. Zhu, J.N. Li, X.J. Ma, Facile synthesis of Mn/N-doped TiO<sub>2</sub> on wood-based activated carbon fiber as an efficient visible-light-driven photocatalyst, *J. Mater. Sci.* 53 (2018) 11671–11683.

[17] Y.J. Zou, J.W. Shi, D.D. Ma, Z.Y. Fan, L. Lu, C.M. Niu, In situ synthesis of C-doped TiO<sub>2</sub>@g-C<sub>3</sub>N<sub>4</sub> core-shell hollow nanospheres with enhanced visible-light photocatalytic activity for H<sub>2</sub> evolution, *Chem. Eng. J.* 322 (2017) 435–444.

[18] A.L. Ortiz, M.M. Zaragoza, J.S. Gutierrez, M.M.D. Paula, V. Collins-Martinez, Silver oxidation state effect on the photocatalytic properties of Ag doped TiO<sub>2</sub> for hydrogen production under visible light, *Int. J. Hydrogen Energy* 40 (2015) 17308–17315.

[19] S.C. Sun, P. Gao, Y.R. Yang, P.P. Yang, Y.J. Chen, Y.B. Wang, N-doped TiO<sub>2</sub> nanobelts with coexposed (001) and (101) facets and their highly efficient visible-light-driven photocatalytic hydrogen production, *ACS Appl. Mater. Interface* 8 (2016) 18126–18131.

[20] L.Q. Yu, M. Li, C.X. Huang, Y.P. Zhang, J.D. He, X.Y. Zhou, H.F. Zhu, Photoelectrochemical properties of N doped black TiO<sub>2</sub> nanotube arrays, *Mater. Lett.* 216 (2018) 239–242.

[21] Y. Cao, Z.P. Xing, Z.Z. Li, X.Y. Wu, M.Q. Hu, X. Yan, Q. Zhu, S.L. Yang, W. Zhou, Mesoporous black TiO<sub>2-x</sub>/Ag nanospheres coupled with g-C<sub>3</sub>N<sub>4</sub> nanosheets as 3D 2D ternary heterojunctions visible light photocatalysts, *J. Hazard. Mater.* 343 (2018) 181–190.

[22] Y. Lu, W.J. Yin, K.L. Peng, K. Wang, Q. Hu, A. Selloni, F.R. Chen, L.M. Liu, M.L. Sui, Self-hydrogenated shell promoting photocatalytic H<sub>2</sub> evolution on anatase TiO<sub>2</sub>, *Nat. Commun.* 9 (2018) 2752.

[23] X.B. Chen, L. Liu, P.Y. Yu, S.S. Mao, Increasing solar absorption for photocatalysis with black hydrogenated titanium dioxide nanocrystals, *Science* 331 (2011) 746–750.

[24] Z. Zhang, W. Jing, X. Tan, T. Yu, J. Ma, High-efficiency photocatalytic performance of Cr-SrTiO<sub>3</sub>-modified black TiO<sub>2</sub> nanotube arrays, *J. Mater. Sci.* 53 (2018) 6170–6182.

[25] S.S. Zhang, S.Q. Zhang, B.Y. Peng, H.J. Wang, H. Yu, H.H. Wang, F. Peng, High performance hydrogenated TiO<sub>2</sub> nanorod arrays as a photoelectrochemical sensor for organic compounds under visible light, *Electrochim. Commun.* 40 (2014) 24–27.

[26] Z.Y. Xiu, Z.P. Xing, Z.Z. Li, X.Y. Wu, X. Yan, M.Q. Hu, Y. Cao, S.L. Yang, W. Zhou, Ti<sup>3+</sup>-TiO<sub>2</sub>/Ce<sup>3+</sup>-CeO<sub>2</sub> Nanosheet heterojunctions as efficient visible -light-driven photocatalysts, *Mater. Res. Bull.* 100 (2018) 191–197.

[27] S.Y. Tan, Z.P. Xing, J.Q. Zhang, Z.Z. Li, X.Y. Wu, J.Y. Cui, J.Y. Kuang, Q. Zhu, W. Zhou, Ti<sup>3+</sup>-TiO<sub>2</sub>/g-C<sub>3</sub>N<sub>4</sub> mesostructured nanosheets heterojunctions as efficient visible-light-driven photocatalysts, *J. Catal.* 357 (2018) 90–99.

[28] L.Y. Shen, Z.P. Xing, J.L. Zou, Z. Li, X.Y. Wu, Y.C. Zhang, Q. Zhu, S.L. Yang, W. Zhou, Black TiO<sub>2</sub> nanobelts/g-C<sub>3</sub>N<sub>4</sub> nanosheets laminated heterojunctions with efficient visible-light-driven photocatalytic performance, *Sci. Rep.* 7 (2017) 41978.

[29] J.Q. Pan, M.Z. You, C.Y. Chi, Z.J. Dong, B.B. Wang, M. Zhu, W.J. Zhao, C.S. Song, Y.Y. Zheng, C.R. Li, The two dimension carbon quantum dots modified porous g-C<sub>3</sub>N<sub>4</sub>/TiO<sub>2</sub> nano-heterojunctions for visible light hydrogen production enhancement, *Int. J. Hydrogen Energy* 43 (2018) 6586–6593.

[30] Z.J. Zhu, Y. Li, C.M. Wang, L.J. Liang, D. Yu, J. Sun, P. Gao, B.J. Liu, Facile synthesis and characterization of Bi<sub>2</sub>MoO<sub>6</sub>/Ag<sub>3</sub>PO<sub>4</sub>/RGO composites with enhanced visible-light-driven photocatalytic activity, *Mater. Lett.* 227 (2018) 296–300.

[31] A.K.R. Police, S.V.P. Vattikuti, K.K. Mandari, M. Chennaiahgari, M.V.P. Sharma, D.K. Valluri, C. Byon, Bismuth oxide cocatalyst and copper oxide sensitizer in Cu<sub>2</sub>O/TiO<sub>2</sub>/Bi<sub>2</sub>O<sub>3</sub> ternary photocatalyst for efficient hydrogen production under solar light irradiation, *Ceram. Int.* 44 (2018) 11783–11791.

[32] R.N. Wang, M. Zu, S.Y. Yang, S.Q. Zhang, W.Y. Zhou, Z.Y. Mai, C.Y. Ge, Y.H. Xu, Y.P. Fang, S.S. Zhang, Visible-light-driven photoelectrochemical determination of Cu<sup>2+</sup> based on CdS sensitized hydrogenated TiO<sub>2</sub> nanorod arrays, *Sens. Actuator B Chem.* 270 (2018) 270–276.

[33] S. Chaguemli, L. Chaperman, S. Nowak, D. Schaming, S. Lau-Truong, P. Decorse, P. Beaunier, C. Costentin, F. Mammeri, S. Achour, S. Ammar, Photoelectrochemical properties of ZnS- and CdS-TiO<sub>2</sub> nanostructured photocatalysts: aqueous sulfidation as a smart route to improve catalyst stability, *J. Photochem. Photobiol. A Chem.* 356 (2018) 489–501.

[34] J. Win, X. Li, S.Y. Yang, X.J. Wang, W.Y. Zhou, Y.P. Fang, S.Q. Zhang, F. Peng, S.S. Zhang, Design and preparation of CdS/H-3D-TiO<sub>2</sub>/Pt-wire photocatalysis system with enhanced visible-light driven H<sub>2</sub> evolution, *Int. J. Hydrogen Energy* 42 (2017) 928–937.

[35] Q. Han, B. Wang, Y. Zhao, C.G. Hu, L.T. Qu, A graphitic-C<sub>3</sub>N<sub>4</sub> "Seaweed" architecture for enhanced hydrogen evolution, *Angew. Chem. Int. Ed. Engl.* 54 (2015) 11433–11437.

[36] J. Liu, Y. Liu, N.Y. Liu, Y.Z. Han, X. Zhang, H. Huang, Y. Lifshitz, S.T. Lee, J. Zhong, Z.H. Kang, Metal-free efficient photocatalyst for stable visible water splitting via a two-electron pathway, *Science* 347 (2015) 970–974.

[37] J. Safaei, H. Ullah, N.A. Mohamed, M.F.M. Noh, M.F. Soh, A.A. Tahir, N.A. Ludin, M.A. Ibrahim, W.N.R.W. Isahak, M.A.M. Teridi, Enhanced photoelectrochemical performance of Z-scheme g-C<sub>3</sub>N<sub>4</sub>/BiVO<sub>4</sub> photocatalyst, *Appl. Catal. B Environ.* 234 (2018) 296–310.

[38] R.N. Wang, J. Yan, M. Zu, S.Y. Yang, X. Cai, Q.Z. Gao, Y.P. Fang, S.S. Zhang, S.Q. Zhang, Facile synthesis of interlocking g-C<sub>3</sub>N<sub>4</sub>/CdS photoanode for stable photoelectrochemical hydrogen production, *Electrochim. Acta* 279 (2018) 74–83.

[39] W. Zhang, L. Zhou, J. Shi, H.P. Deng, Synthesis of Ag<sub>3</sub>PO<sub>4</sub>/G-C<sub>3</sub>N<sub>4</sub> composite with enhanced photocatalytic performance for the photodegradation of diclofenac under visible light irradiation, *Catalysts* 8 (2018) 45.

[40] J. Li, C.B. Cao, H.S. Zhu, Synthesis and in vitro antieoagulation activity of hollow carbon nitride microspheres, *Diam. Relat. Mater.* 16 (2007) 359–363.

[41] S.B. Kokane, R. Sasikala, D.M. Phase, S.D. Sartale, In<sub>2</sub>S<sub>3</sub> nanoparticles dispersed on g-C<sub>3</sub>N<sub>4</sub> nanosheets: role of heterojunctions in photoinduced charge transfer and photoelectrochemical and photocatalytic performance, *J. Mater. Sci.* 52 (2017) 7077–7090.

[42] F.Y. Xu, J.J. Zhang, B.C. Zhu, J.G. Yu, J.S. Xu, CuInS<sub>2</sub> sensitized TiO<sub>2</sub> hybrid nanofibers for improved photocatalytic CO<sub>2</sub> reduction, *Appl. Catal. B Environ.* 230 (2018) 194–202.

[43] H. Chen, Z.G. Gu, S. Mirza, S.H. Zhang, J. Zhang, Hollow Cu-TiO<sub>2</sub>/C nanospheres derived from a Ti precursor encapsulated MOF coating for efficient photocatalytic hydrogen evolution, *J. Mater. Chem. A Mater. Energy Sustain.* 6 (2018) 7175–7181.

[44] C.Q. Zhu, B.A. Lu, Q. Su, E.Q. Xie, W. Lan, A simple method for the preparation of hollow ZnO nanospheres for use as a high performance photocatalyst, *Nanoscale* 4 (2012) 3060–3064.

[45] L.Y. Lin, S. Kavadiya, B.B. Karakocak, Y. Nie, R. Raliya, S.T. Wang, M.Y. Berezin, P. Biswas, ZnO<sub>1-x</sub>carbonydots composite hollow spheres: facile aerosol synthesis and superior CO<sub>2</sub> photoreduction under UV, visible and near-infrared irradiation, *Appl. Catal. B Environ.* 230 (2018) 36–48.

[46] L.B. Xiao, R.B. Lin, J. Wang, C. Cui, J.Y. Wang, Z.Q. Li, A novel hollow-hierarchical structured Bi<sub>2</sub>WO<sub>6</sub> with enhanced photocatalytic activity for CO<sub>2</sub> photoreduction, *J. Colloid Interface Sci.* 523 (2018) 151–158.

[47] Z.Y. Jiang, J.Q. Pan, B.B. Wang, C.R. Li, Two dimensional Z-scheme AgCl/Ag/CaTiO<sub>3</sub> nano-heterojunctions for photocatalytic hydrogen production enhancement, *Appl. Surf. Sci.* 436 (2018) 519–526.

[48] S.Y. Chou, C.C. Chen, Y.M. Dai, J.H. Lin, W.W. Lee, Novel synthesis of bismuth oxyiodide/graphitic carbon nitride nanocomposites with enhanced visible-light photocatalytic activity, *RSC Adv.* 6 (2016) 33478–33491.

[49] Q. Wei, Y. Wang, H.Y. Qin, J.M. Wu, Y.F. Lu, H.Z. Chi, F. Yang, B. Zhou, H.L. Yu, J.B. Liu, Construction of rGO wrapping octahedral Ag-Cu<sub>2</sub>O heterostructure for enhanced visible light photocatalytic activity, *Appl. Catal. B Environ.* 227 (2018) 132–144.

[50] S.B. Kokane, R. Sasikala, D.M. Phase, S.D. Sartale, In<sub>2</sub>S<sub>3</sub> nanoparticles dispersed on g-C<sub>3</sub>N<sub>4</sub> nanosheets: role of heterojunctions in photoinduced charge transfer and photoelectrochemical and photocatalytic performance, *J. Mater. Sci.* 52 (2017) 7077–7090.

[51] D.J. Martin, P.J.T. Reardon, S.J.A. Moniz, J.W. Tang, Visible light-driven pure water splitting by a nature-inspired organic semiconductor-based system, *J. Am. Chem. Soc.* 136 (2014) 12568–12571.

[52] Y.K. Hsu, C.H. Yu, Y.C. Chen, Y.G. Lin, Synthesis of novel Cu<sub>2</sub>O micro/nanostructural photocathode for solar water splitting, *Electrochim. Acta* 105 (2013) 62–68.

[53] J. Schneider, M. Matsuoka, M. Takeuchi, J.L. Zhang, Y. Horiuchi, M. Anpo, D.W. Bahnemann, Understanding TiO<sub>2</sub> photocatalysis: mechanisms and materials, *Chem. Rev.* 114 (2014) 9919–9986.

[54] N.A. Deskins, R. Rousseau, M. Dupuis, Localized electronic states from surface hydroxyls and polarons in TiO<sub>2</sub>(110), *J. Phys. Chem. C* 113 (2009) 14583–14586.